Self-regulated complexity in neural networks

Eyal Hulata, Vladislav Volman, Eshel Ben-Jacob
School of Physics and Astronomy,
Raymond & Beverly Sackler Faculty of Exact Sciences,
Tel-Aviv University, Tel-Aviv 69978, Israel
Corresponding author: Eshel Ben-Jacob,
email: eshel@tamar.tau.ac.il,
Telephone no.: 972-3-6407845, Fax: 972-3-6425787

April 16, 2005

Key words: structural complexity, neural network, temporal organization, self regulation, neuroinformatics, dynamical systems, wavelet packet, time-frequency analysis

Abstract

Recordings of spontaneous activity of *in-vitro* neuronal networks reveal various phenomena on different time scales. These include synchronized firing of neurons, bursting events of firing on both cell and network levels, hierarchies of bursting events etc. These findings suggest that networks' natural dynamics are self-regulated to facilitate different processes on intervals in orders of magnitude ranging from fractions of seconds to hours. Observing these unique structures of recorded time-series give rise to questions regarding the diversity of the basic elements of the sequences, the information storage capacity of a network and the means of implementing calculations.

Due to the complex temporal nature of the recordings, the proper methods of characterizing and quantifying these dynamics are on the

time-frequency plane. We thus introduce time-series analysis of neuronal network's synchronized bursting events applying the wavelet packet decomposition based on the Haar mother-wavelet. We utilize algorithms for optimal tiling of the time-frequency plane to signify the local and global variations within the sequence. New quantifying observables of regularity and complexity are identified based on both the homogeneity and diversity of the tiling [1]. These observables are demonstrated while exploring the regularity-complexity plane to fulfill the accepted criteria (yet lacking an operational definition) of Effective Complexity. The presented question regarding the sequences' capacity of information is addressed through applying our observables on recorded sequences, scrambles sequences, artificial sequences produced with similar long-range statistical distributions and on outputs of neuronal models devised to simulate the unique networks' dynamics.

Self-regulated complexity

Diverse natural systems, biotic and abiotic alike, can exhibit self-organization of complex structures and dynamics [2, 3, 4, 5, 6, 7, 8, 9, 10, 11, 12, 13]. Higher complexity elevates their self-plasticity and flexibility which, in turn, impart them better adaptability to external stimuli and imposed tasks [2, 5, 13]. It has been suggested that the referred biotic complexity is self-regulated and generated via autonomous utilization of internal means, hence the term self-regulated complexity [13]. If correct, this special nature of biotic complexity should be manifested in some observable features of the dynamical behavior. This infer that in principle, with proper observables, it should be possible to distinguish between biotic and non autonomous abiotic complexities.

Therefore, understanding this linkage and the behavioral motifs of such complex adaptive systems requires understanding of complexity. However, despite the quest for an operational measure, this concept is still blurred and intuitive,

with no agreed definition [5, 6, 7, 14, 9, 11, 12, 13]. This state of affairs might stem from the intermingled common use of the term to describe different notions [14, 6, 11, 12, 13]. To avoid the confusion, we adapted the distinction between structural (configurational) and operational (functional) complexity [14, 11, 13] and present a new measurable definition of the former.

Hints about self-regulation in cultured networks

Our *in-vitro* neuronal networks were spontaneously formed from a mixture of cortex neurons and glia cells homogeneously spread over a lithographically specified area [15]. Consequently, the spread cells turned into a network by sending dendrites and axons, to form synaptic connections between neurons [16, 17, 18]. Although the above described self-wiring process is self-executed with no externally provided guiding stimulations or chemical cues, a relatively intense dynamical activity is spontaneously generated within several days. The activity is marked by the formation of synchronized bursting events (SBEs), each in short ($100 - 400 msecs$) time windows during which most of the recorded neurons participate in relatively rapid firing. For the analysis of the temporal ordering of the events it is convenient to convert the recorded activity into a binary sequence, whose "1"s, correspond to the SBEs [18]. An illuminating example of the formation of such a binary sequence is shown in Fig.1. We have shown that the SBEs show long time correlations, and for some networks, clear hierarchical temporal ordering is observed (i.e. bursts of SBEs, bursts of bursts of SBEs, up to four detectable hierarchical levels)[16]. This behavior is presented in Fig.2. Put together, the above observations motivated us to assume that the spontaneous activity of cultured networks, might be self-regulated despite the artificial nature of their construction. Such self-regulation can be executed via neuronal internal autonomous means which are self-activated by the neurons. Or even more likely, they are co-activated by glia cells (with their own complementary regulatory means) which are coupled to the neurons [19, 20, 21, 22].

Looking for quantified observables of self-regulated complexity

Guided by the notion of self-regulated complexity (vs. abiotic-like non-autonomous complexity), we set to develop proper observables for distinguishing between these possibilities. To proceed, we observe the features of a recorded sequence such as presented in Fig.2. The recorded sequence is characterized by large local and global temporal variations. Namely, at each temporal location, there are large frequency (density of SBEs) variations when looking at time windows of different widths. These local variations vary from place to place along the sequence.

Another illuminating example of a sequence with complex temporal organization is provided by the recorded time series of neuronal activity such as the one presented in Fig. 3 [16]. We illustrate in Fig.3 that shuffling (random reordering of the intervals) alters the temporal ordering of the original sequence, yet preserves the same statistical scaling properties. As suggested in [16], through out our research of neuronal recordings, we approximated the statistical behavior of our recordings using the Lévy distribution [1] [24, 25, 23, 26].

Once again, it is visualized that the temporal structure is composed of time segments of dense activity (bursts) separated by time intervals of relatively sparse activity which infer local and global variations. These characteristic features

[1] The Lévy distribution $P_{\alpha\gamma}$ of X is given by $P_{\alpha\gamma}(X) = \frac{1}{\pi}\int_0^\infty exp(-\gamma q^\alpha)cos(qX)dq$ where $0 < \alpha \leq 2$ is the index of stability, which determines the long tail decay of the distribution, and $\gamma > 0$ is a scale factor, which determines the location of the bending point of the Lévy distribution. Special cases of the Lévy distribution are the Gaussian distribution ($\alpha = 2$) and the Cauchy distribution ($\alpha = 1$). The Lévy statistics is a family of random distribution that have three important mathematical properties:

1. These distributions are stable. That is, the sum of random variables of this kind also has stable distribution.

2. The asymptotic behavior for large values of X is a power-law behavior. That is: $P_L(|X|) \sim |X|^{-(1+\alpha)}$ for large values of X. The moments of the distribution are deeply affected by this property [23]. Specifically, all moments of the distribution diverge for $\alpha < 2$. Thus, all non Gaussian stable stochastic processes do not have characteristic time scale due to the fact that the variance is infinite.

3. Lévy distribution resigns in the Generalized Central Limit Theorem. According to the classical Central Limit Theorem, the normalized sum of independent and identically distributed random variable with a finite variance converges to a normal distribution. The Generalized Central Limit Theorem proclaims that if the finite variance assumption is to be dropped, the only possible resulting limits are stable, i.e. Lévy distributions.

which are not invariant under scrambling (Fig. 3) might provide the sequence a template for the encoding of information as we comment at the end. They are also the structural traits that cause their appearance to look complex.

Guided by this awareness and the previously mentioned special temporal features of the recorded sequences, we set the following requirements from our observables: 1. To associate the sequence regularity with the uniformity in the time-frequency (rates) relative resolutions rather than with the statistics of the temporal ordering. The former refers to the relative resolution required to capture maximal information about the observed variations. 2. To associate the sequence complexity with the local and global variations in the required relative resolutions, instead of the directly observed local and global frequency variations. 3. To evaluate significantly lower values of complexities to the recorded sequences after they are shuffled while keeping similar regularity regardless of shuffling. 4. To be able to distinguish between the dynamical behaviors of different systems by their distinct positions on the complexity-regularity plane. 5. To be able to handle sequences with hierarchical temporal organizations.

Representation at the time-frequency plane

To retain information about both temporal locations and frequency variations, we first transform the sequence into a presentation in its corresponding time-frequency domain utilizing the Wavelet Packets Decomposition (WPD)

The WPD decomposes a signal $f(t)$ into a set of levels, each with a unique time-frequency resolution. The packets are are a set of orthogonal localized functions. Localized, in the sense that each has a definite support of both the time and frequency domain. In Fig. 4 we present an example the levels of decomposition for the type of wavelet packets used for this paper - packets produced from the Haar mother wavelet [27, 28, 29].

Next, we would like to extract at each temporal position (say the i-th element of the sequence) information about the activity rates (frequencies) for all available

time windows centered around this location. For a sequence of N_{bin} elements, the relevant time windows range from $\Delta t_{min} \equiv 1$ (in units of the basic recording time width) to $\Delta t_{max} \equiv N_{bin}$. That is, we would like to extract information about N_{bin} time windows at each of the N_{bin} locations of the sequences. However, such N_{bin}^2 matrix for a sequence of only N_{bin} elements must contain redundant information (i.e. over-complete representation of the recorded sequence). In order to avoid such redundancy, only N_{bin} locations on the time-frequency domain are allowed to be selected, subject to the uncertainty constraint between time and frequency resolutions, $\Delta t \Delta f = 1$. Since there are also N_{bin} frequency bands, from $\Delta f_{min} = 1$ to $\Delta f_{max} = N_{bin}$ it implies that each location can be assigned a local relative resolution $\Delta t / \Delta f$ out of $N_R = 1 + log_2(N_{bin})$ possible ratios (for simplicity, N_{bin} of the sequences considered here are in factors of 2).

It is convenient to illustrate both constraints as tiling of the time-frequency domain with N_{bin} rectangles, each with its own aspect ratio (height Δf and width Δt) representing the relative resolutions in time and frequency, and equal area $\Delta t \Delta f = 1$. In other words, the WPD algorithm allows partitioning (tiling) of the domain into rectangles of different aspect ratios. Each possible combination of N_{bin} non-overlapping rectangles that geometrically covers the entire domain can serve as a complete basis that spans the recorded sequence on its corresponding time-frequency domain.

Selecting the Best Tiling

The next challenge is to select, out of all possible tilings, the one which is most efficient in extracting from the recorded sequence the features of interest [29, 30]. Here we are interested in a method that will generate for the recorded sequence and its shuffled one distinct tilings, as illustrated in Fig.5. We follow the approach of Thiele and Villemoes [30], which is inspired by the notions of global Shannon information or Entropy minimization. The idea is to select the combination of rectangles that can capture most efficiently the information about

local and global variations in the sequence temporal ordering. In other words, we aim to select a tiling that minimizes the sum of the cost function M [31, 29, 30]:

$$M_n = -q_n log(q_n) \tag{1}$$

where q_n is the normalized energy of the signal on the n^{th} rectangle. The global measure M - the summation of M_n over the N_{bin} rectangles - is utilized for selecting the Best Tiling. The algorithm developed by Thiele and Villemoes was proved to minimize M [30].

In Fig. 6 we demonstrate the concept of best tiling of the time-frequency plain. The temporal barcode bellow is composed of three segments: In the middle, we present a sequence of SBEs from an *in-vitro* neuronal network [16]. To the left, we present the same sequence after we have shuffled the order of the intervals. To the right, we present a periodic signal. On top, the time-frequency plane is presented by a set of rectangles, whose color represent the energy content within each of the time-frequency rectangles. The tiling of the periodic region is straight-forward: since the events are separated by equal intervals, there is a distinct energetic frequency band, and the rest of the time-frequency plane has no energy content. The neuronal sequence in the middle has much more variety within the tiling. There is a mixture of rectangles with different aspect ratios one beside the other. On the other hand, the randomly shuffled sequence on the left has a more homogeneous tiling, where adjacent tiles tend to be similar. Further ahead, we shall define measures that can quantify this effect.

In Fig. 7 we present the tiling of the recorded binary sequence and the shuffled sequence of Fig. 3. Note how the tilings emphasize the differences in internal structure between the recorded sequence and the randomly ordered one.

Regularity measure of a sequence

As originally pointed out by Hubermann and Hogg [2], in order to define the complexity of a sequence, its regularity must first be defined. The regularity is a measure of the relative location of the sequence on the abscissa between complete

random (disordered) signals on one edge (regularity=0) and purely periodic (ordered) ones on the other edge (regularity=1). Various measures for the sequence regularity have been suggested, such as the Algorithmic Information Content [5, 7]. We propose that the definition of the regularity should go hand in hand with the definition of the sequence structural complexity, since the latter has to be a functional of the former.

The idea is to associate the sequence regularity with the uniformity of its corresponding time-frequency domain, namely, with the uniformity of its rectangle distribution. The latter represents the distribution of the local relative resolutions in time and frequency as selected by the best tiling for extracting maximal information from the sequence.

From physics perspective, a tiled domain (Fig. 3,5) can be viewed as a magnetic material with the rectangles representing its local magnetizations. With this picture in mind, we first relate the local relative resolution of each rectangle n with its aspect ratio $(\Delta t/\Delta f)$ by:

$$R_n \equiv \frac{log_2(\Delta t/\Delta f)}{log_2(N_{bin})} \tag{2}$$

Defined this way, R_n (the analogue of a local magnetization) is assigned positive values for rectangles with higher frequency resolution (lower Δf) and negative values for those with higher time resolution. Consequently, it has the lowest average absolute values for a signal with a wide distribution of tiles and the highest values for signals with a large majority of tiles with high aspect ratios (Fig. 8). The normalization of R_n by the logarithm of the maximal aspect ratio N_{bin} makes that $-1 \leq R_n \leq 1$. Therefore, we propose the regularity measure RM to be defined as the average value of R_n (the analogue of the total magnetization):

$$RM \equiv \frac{1}{N_{bin}} \sum_{n=1}^{N_{bin}} R_n \tag{3}$$

As demonstrated in Fig.8, $RM \cong 0$ for completely disordered sequences, i.e. sequences with Gaussian distribution of intervals, and $RM \cong 1$ for purely regular

ones, i.e strings of one kind of interval. As will be shown later, artificial sequences constructed from the periodic and the random ends towards the center meet around $RM = 0.5$. RM can also assign negative values for under-dense (sparse) sequences in which the number of intervals is smaller than $\sqrt{N_{bin}}$. Such sequences are not considered here.

Variation factors and Structural Complexity

The regularity observable represents the uniformity of the time-frequency plane. We now set to define additional complementary observables associated with the local and global variability of the plane. Local variability will be related to the amount of diversity within the tiling within local segments of the sequence. Global variability will be related to the amount of variation between the tilings among the different segments.

Thus, we begin by segmenting the sequence into words. We quantify the amount of local variation within each word using an observable named **variation factor (VF)**. For each word l, we define the variation factor of word to be:

$$VF_l = \left(\frac{N_E(l) - \overline{N_E}}{\overline{N_E}}\right)\frac{\sum_{n,m} |R_n - R_m| \cdot \Theta(q_n \cdot q_m)}{\sum_{n,m} \Theta(q_n \cdot q_m)} \tag{4}$$

where the sum is over all neighboring rectangles n, m. $N_E(l)$ is the number of events (and also intervals) detected within the l-th word, and $\overline{N_E}$ is an average over different words of the same length as the l-th one. $\Theta(x)$, is the heavyside function; $\Theta(0) = 0$ and $\Theta(x \neq 0) = 1$.

Finally, we quantify the global variability of the sequence using the variance of the variation factors between the sequence words. For a sequence segmented into N_ω words, we thus define the **structural complexity (SC)** observable to be:

$$SC \equiv var(VF) \equiv \frac{1}{N_\omega}\sum_{l=1}^{N_\omega}(VF_l - \overline{VF})^2 \tag{5}$$

Exploring the complexity plane with test Lévy sequences

In order to test these definitions by relating them to a concrete example, we first devised a method to construct a family of binary time series, spanning from completely random (disordered) sequences to purely periodic (ordered) ones in the following manner. For the completely random sequence, the intervals between the events (inter-event intervals, or IEI) are drawn from a normal distribution (taking only positive increments). For the purely periodic sequence, the IEIs are all equal to the period of the signal. Next, we proceed from these two extremes to the center. From the regular edge, we start with a very narrow Lévy distribution [16, 23, 24, 25] of the IEI centered around the period of the sequence. Then, the distribution is modified into a wider one and with a tail shape changing from exponential to power law decay. From the random edge, we perform the same procedure but starting with a distribution centered around zero.

The statistical characteristics of the Lévy distribution are controlled by three parameters: α controls the tail decay of the statistics, γ controls the width of the distribution and δ is the most probable event. In our case, δ related to the period of the sequence, while α and γ relate to the variability of the sequence. In order to gain better understanding of the relation between the statistical properties of the sequences (e.g. α, γ and δ) and their locations on the regularity-complexity plane, we utilized artificially constructed families of sequences with different Lévy parameters.

The construction of an artificial sequence is as follows. We draw a set of numbers out of a Lévy distribution generator with parameters α, γ and δ. This set is then rounded and used as intervals between adjacent events in a sequence. This sequence is considered a *realization* of the distribution. Naturally, there could be variations between different realizations of the same Lévy distribution. Hence, for each set of Lévy parameters, we have constructed 10-20 realizations and calculated RM and SC for each of them. We thus use $\overline{RM}$ and $\overline{SC}$ as the Regularity and Structural Complexity, and the deviations between the individual

values as the error bars ($< 13\%$). It is important to point out that shuffling the intervals of an artificial realization simply produces another realization of the same Lévy distribution. We have noticed that there was no difference between $\overline{RM}$ and $\overline{SC}$ of the original and shuffled artificial realizations (within error deviations). Our procedure enables us to construct families of binary sequences, such that each family contains sequences that cover the entire range from disordered to purely periodic ones, as illustrated in the characteristics shown in Fig.9. Each family of sequences for a given α is composed of one branch on the random side ($RM < 0.5$) for $\delta =$ "0" (minimum of one bin separation between events). On the regular side ($RM > 0.5$), each family has a unique branch for every $\delta \neq$ "0". The branches are spanned by varying γ and they all meet for $\gamma >> \delta$ at a location on the border between the random and regular sides and at relatively higher complexity (as shown in detail in Fig.9).

As demonstrated, the above measure of complexity successfully fulfills the commonly agreed criteria mentioned earlier [2, 5]. We emphasize though that the interpretation of the accepted criteria [2, 5] should be taken with caution. Not all signals can and should be fitted on a single universal curve, but rather fill the entire complexity plane ($SC - RM$ plane). Only a continuous family of signals spanning from random to periodic (as was produced here) can result a fully extended curve like the one shown in Fig. 9. Different families of sequences will yield different curves or clusters.

Experimental findings: utilizing the complexity plane in search for self-regulation in neuronal recordings

As shown, families of artificially constructed sequences exhibit very rich characteristics on the regularity-complexity plane. These characteristics map can be utilized as a "grid" while analyzing sequences of unknown Lévy parameters or, as in our case, sequences originating from a recorded biotic system.

We are now ready to identify features presumably related to self-regulation

motifs of biotic systems. As stated previously, using the term self-regulation we claim that the temporal structures of neuronal networks are not random or arbitrary. Rather, they originate from internal dynamics and internally-stored means of control (on individual cell level, neuron-glia dynamics, global chemical and electric dynamics on the network level, etc.).

In Fig. 10 we show typical examples of the evaluated regularity-complexity values for recorded sequences of *in-vitro* neuronal networks. We compare their values with those of the randomly shuffled sequences from the same recordings. Also shown are the values of corresponding artificially constructed sequences with matching α, γ and δ parameters as the recorded and shuffled sequences. While these three types of sequences have very similar regularity, the recorded ones have significantly higher complexity then the shuffled sequences - as is clearly seen in the figure. The large circles are well above the different shuffled segments represented by the smaller circles ($30-45\%$ higher). Moreover, the complexity of the shuffled sequences are very similar to that of the artificial sets with matching Lévy parameters (represented by full circles) - the typical difference is within the natural deviation among different realizations. Clearly, the two presented examples have some probability (albeit low) of being accidental. However, it is repeatedly obtained for all the recorded sequences we tested (we have tested a few tens of sequences from several different cultured networks of different sizes and different number of neurons from 50 to 1,000,000). We propose that the results described above, do provide a hint that the observed complexity is self-regulated. In this regard, we emphasize that for abiotic (non autonomous) activity we found that the recorded and shuffled sequences exhibit similar values of complexities which are also similar to that of the artificially constructed ones.

Testing the validity of the analysis on simulation sequences

We wish to further strengthen our argument regarding the ability to detect the self-regulation motifs of biotic systems. We have thus cross-compared the

behavior of the neuronal sequences to the behavior of sequences from a simulated model. These simulated sequences are time-series of the dynamical synapse and soma model, recently introduced by Volman et.al. [32, 33]. The neurons in our model network are described by the two-variables Morris-Lecar model [34, 32, 33], which partially takes into account the dynamics of membrane ion channels. Briefly, the equations describing the neuronal dynamics are:

$$\begin{aligned} \dot{V} &= -I_{ion}(V,W) + I_{ext}(t) \\ \dot{W}(V) &= \phi \frac{W_\infty(V) - W(V)}{\tau_W(V)} \end{aligned} \tag{6}$$

In the above equations, $I_{ion}(V,W)$ represents the contribution of the internal ionic Ca^{2+}, K^+ and leakage currents, with their corresponding channel conductivities g_{Ca}, g_K and g_L being constant:

$$I_{ion}(V,W) = g_{Ca} m_\infty(V)(V - V_{Ca}) + g_K W(V)(V - V_K) + g_L(V - V_L) \tag{7}$$

The additional current I_{ext} represents all the external current sources stimulating the neuron. These might be, for example, synapse-related signals received from other neurons, glia-derived currents, currents resulting from artificial stimulations, or any noise sources. The neurons in the model network exchange action potentials via the activity-dependent synapses, as first described by Tsodyks et.al. [35].

The output of the simulation is a time-series of action potentials for each model-neuron, similar in form and characteristic time-scales as our *in-vitro* neuronal recordings (and as presented in Fig. 1). Moreover, we have shown in [32, 33] that our model forms SBEs and the inter-SBEs intervals follow similar Lévy statistics as our *in-vitro* neuronal recordings. Thus, the simulated sequence are analyzed as the neuronal recording - SBEs are identified and a binary sequence is formed where each bin represents an interval of $400msec$.

Fig. 10 presents the RM and SC values assigned to the simulated binary sequences from two different simulations. We also present the values assigned for shuffled sequences, as we have done for neuronal recording. Note that for

the two simulated examples the simulation values are not higher that the shuffled sequences, implying that there is no hidden internal structure within the sequences.

However, we must stress that we have found larger sensitivity to the bin width in the simulated sequences than for neuronal sequences. In other words, for bins of $800msec$ we got different values with large variation than for $400msec$. This may imply that in turn there are internal structures in different time scales to be further studied.

Hierarchical structural complexity

Sequences with hierarchical organization are more complex and pose additional challenge, especially when each level has its own specific organization and characteristic time scale. Our new approach bears the promise that it can be extended to measure the complexity of hierarchical temporal organization as well. We have already found how to evaluate the time scale of a higher level from the temporal organization of a given level using our method. As shown in Fig. 11, for hierarchical sequences with a given basic time scale, the variance of the variation factor exhibits a maximum at a specific sequence segmentation, i.e. division into words of specific length. This segmentation length defines the time scale (τ_{bin}) of the next level. Therefore, the regularity measure and structural complexity of the higher level depend also on the properties of the lower level. This realization hints about the way to evaluate the structural complexity of a hierarchical sequence using a self-consistent (solvability) principle between levels, as will be presented elsewhere [36].

Conclusions

We have shown that our novel observables of regularity and structural complexity fulfill the following: 1. To follow the foreseen characteristic of an effective complexity measure, as presented in [2, 5]. 2. To assign a significantly lower

value to a biotic sequence after its intervals have been shuffled. Our work was performed on binary sequences created from the recording of *in-vitro* neuronal networks. We have compared the complexity values of these sequences with the values obtained for sequences generated by shuffling the recorded inter-event intervals. We have performed the same analysis on simulated sequences produced by our model of neuronal dynamics and on artificial sequences constructed to have the same Lévy statistic parameters. While simulated and artificial sequence have similar structural complexity values regardless of shuffling, the neuronal sequences are assigned much higher values of structural complexity than the shuffled sequences (Fig.10). We argue that this imply that for a biotic sequence, the order of the events bears information or provides a template for coding of information. By shuffling of the intervals, the information encoded in the order of intervals is lost or at least reduced.

We propose that the high complexity exhibited in the *in-vitro* neuronal network is consistent with their free and spontaneous activity. Such isolated networks should be ready to have the full extent of possible templates to sustain the different neuro-informatics tasks upon being connected to other networks. Therefore, complex activity is required to elevate their self-plasticity and flexibility that impart them better adaptability and efficiency to communicate with other networks and to perform imposed tasks as needed [13]. In this regard, it would be important to test the complexity of linked *in-vitro* networks and to compare between recorded activity from different functional locations of the brain.

Moreover, in upcoming work, we intend to further show that these observables are useful in generating curves and clusters in the regularity-complexity plane following the dynamics of the biotic system. For example, during the development of a network, the complexity values grow as well as the distance between the complexities of the recorded sequences vs. the shuffled sequences.

Finally, we emphasize that our new method is introduced here in connection with binary time series (temporal sequences) merely for the ease of presentation.

Clearly this approach can be extended to general temporal signals and is applicable to spatial series and other informatic strings such as DNA sequences and written text.

Acknowledgments

We benefited from illuminating discussions with N. Tishby, R. Segev, I. Baruchi and N. Raichman. We are most thankful for collaborative work with A. Ayali, E. Fuchs and A. Robinson on application of the structural complexity ideas to the "Contextual regularity and complexity of neuronal activity" [37] . E. Hulata thanks A. Averbuch and R. Coifman for inspiring conversations about the tiling of wavelet packets and basis selections. E. Ben-Jacob thanks S. Edwards, I. Procaccia, P. Hohenberg and W. Kohn for illuminating conversations, especially about autonomous vs. non autonomous systems. The studies presented here have been supported in part by the Adams supercenter, the Kodesh institute and a grant from the Israeli Science Foundation (ISF).

References

[1] E. Hulata, I. Baruchi, R. Segev, Y. Shapira, and E. Ben-Jacob. Self-regulated complexity in cultured neuronal networks. *Phys.Rev.Lett.*, 92:198181–198104, 2004.

[2] B.A Hubermann and T. Hogg. Complexity and adaptation. *Physica D*, 22:376, 1986.

[3] E. Ben-Jacob and P. Garik. The formation of patterns in non equilibrium growth. *Nature*, 33:523–530, 1990.

[4] M. Waldrop. *Complexity.* Simon & Schuster, 1993.

[5] M. Gell-Mann. *The Quark and the Jaguar.* FREEMAN, N.Y., 1994.

[6] J. Horgan. From complexity to perplexity. *Sci. Am.*, 272:74–79, 1995.

[7] R. Badii and R. Politi. *Complexity, Hierarchical Structures and Scaling in Physics*. Cambridge University Press, 1997.

[8] Complexity volume. *Science*, 284, 1999.

[9] N. Goldenfeld and L.P. Kadanoff. Simple Lessons from Complexity. *Science*, 284:87–89, 1999.

[10] M.A. Jimenez-Montano et al. Measures of complexity in neural spike-trains of the slowly adapting stretch receptor organs. *Biosystems*, 58:117–124, 2000.

[11] E. Ben-Jacob and H. Levine. The artistry of Nature. *Nature*, 409:985–986, 2001.

[12] T. Vicsek. The bigger picture. *Nature*, 418:131, 2002.

[13] E. Ben-Jacob. Bacterial Self-Organization: co-enhancement of complexification and adaptibility in a dynamic environment. *Phil.Trans.Roy.Soc. London*, A 361:1283–1312, 2003.

[14] E. Ben-Jacob. From snowflake formation to growth of bacterial colonies II:Cooperative formation of complex colonial patterns. *Contemporary Physics*, 38:205, 1997.

[15] Dissociated cultures of cortical neurons from one-day-old Charles River rats were prepared and maintained as described previously [38, 16]. The cultures were maintained in growth conditions at $37^o c$ with $5\%CO_2$ and 95% humidity prior to and during measurements. Non-invasive extracellular recordings were taken from an array of 60 substrate-integrated micro-electrodes (MEA-chip, Multi-Channel Systems, Germany [39]). The signal was amplified (Multi-Channel Systems) and digitized (Alpha Omega Engineering, Israel). Off-line spike-sorting of the extracellular recordings were performed by our Wavelet Packets method [40, 41]. An average of 30 different neurons are typically identified in a recording. SBEs are identified and analized as

described in [38, 16, 18]. The typical temporal width of an SBE is 100msec and the typical temporal interval between consequtive SBEs is 1sec.

[16] R. Segev et al. Long term behavior of lithographically prepared in vitro neural networks. *Phy. Rev. Lett.*, 88:1181021–1181024, 2002.

[17] R. Segev, M. Benveniste, Y. Shapira, and E. Ben-Jacob. Formation of electrically active clusterized neural networks. *Phys.Rev.Lett.*, 90:168101/1–4, 2003.

[18] R. Segev, I. Baruchi, E. Hulata, and E. Ben-Jacob. Hidden neuronal correlations in cultured neuronal networks. *Phys.Rev.Lett.*, 92:1181021–1181023, 2004.

[19] P.R. Laming et al. Neuronal-glial interactions and behaviour. *Neuroscience and Biobehavioral Reviews*, 24(3):295–340, 2000.

[20] C.E. Stout at al. Intercellular calcium signaling in astrocytes via ATP release through connexin hemichannels. *J.Bio.Chem.*, 277:10482–10488, 2002.

[21] M. Zonta and G. Carmignoto. Calcium oscillations encoding neuron-to-astrocyte communication. *J. of Physiology*, 96:193–198, 2002.

[22] M.C. Angulo, A.S. Kozlov, S. Charpak, and E. Audinat. Glutamate released from glial cells synchronizes neuronal activity in the hippocampus. *The Journal of Neurosci.*, 24(31):6920–6927, 2004.

[23] R.N. Mantegna and H.E. Stanley. Scaling behavior in the dynamics of an economic index. *Nature*, 376:46–49, 1995.

[24] C.K. Peng, J. Mietus, J.M. Hausdorff, S. Havlin, H.E. Stanley, and A.L. Goldenberger. Long-range anticorrelations and non-gaussian behavior of the heartbeat. *Phys. Rev. Lett.*, 70:1343–1346, 1993.

[25] M.F. Shlesinger, G.M. Zaslavsky, and J. Klafter. Strange kinetics. *Nature*, 363:31, 1993.

[26] H.E. Stanley et al. Statistical physics and physiology: Monofractal and multifractal approaches. *Physica A*, 270:309–324, 1999.

[27] R.R. Coifman, Y. Meyer, and M.V. Wickerhauser. *Wavelet analysis and signal processing. in: Wavelets and their applications.* Jones and Barlett, Boston, 1992.

[28] R.R. Coifman and M.V. Wickerhauser. Wavelets and Adapted Waveform Analysis. A Toolkit for Signal Processing and Numerical Analysis. *Proc. Symp. in Applied Mathematics*, 47:119–153, 1993.

[29] S. Mallat. *A wavelet tour of signal processing.* Academic Press, 1998.

[30] C. Thiele and L. Villemoes. A fast algorithm for adapted Walsh bases. *Appl. Comp. Harm. Anal.*, 3:91–99, 1996.

[31] R.R. Coifman and M.V. Wickerhauser. Entropy-based Algorithms for Best Basis Selection. *IEEE Trans. Infor. The.*, 38(2):713–718, 1992.

[32] V. Volman, I. Baruchi, E. Persi, and E. Ben-Jacob. Generative modelling of regulated dynamical behavior in cultured neuronal networks. *Physica A*, 235:249–278, 2004.

[33] V. Volman, I. Baruchi, and E. Ben-Jacob. Manifestation of function-follow-form in cultured neuronal networks. *submitted to Physical Biology*, 2005.

[34] C. Morris and H. Lecar. *Biophys Journal*, 35:193–213, 1981.

[35] M. Tsodyks, A. Uziel, and H. Markram. *The Journal of Neurosci*, 20, 2000.

[36] E. Hulata, R. Segev, Y. Shapira, and E. Ben-Jacob. Hierarchic Temporal Bar-Codes and Structural Complexity in Neuronal Networks Activity. *in preparation.*

[37] A. Ayali, E. Fuchs, Y. Zilberstein, A. Robinson, O. Shefi, E. Hulata, I. Baruchi, and E. Ben-Jacob. Contextual regularity and complexity of neuronal activity: from stand-alone cultures to task-performing animals. *Complexity*, 9:25–32, 2004.

[38] R. Segev, Y. Shapira, M. Benveniste, and E. Ben-Jacob. Observations and Modeling of Synchronized Bursting in 2D Neural Networks. *Phy. Rev. E*, 64:011920, 2001.

[39] U. Egert, B. Schlosshauer, S. Fennrich, W. Nisch, M. Fejtl, T. Knott, T. Muller, and H. Hammerle. A novel organotypic long-term culture of the rat hippocampus on substrate-integrated multielectrode arrays. *Brain. Res. Proto.*, 2:229–242, 1998.

[40] E. Hulata, R. Segev, Y. Shapira, M. Benveniste, and E. Ben-Jacob. Detection and sorting neural spikes using wavelet packets. *Phy. Rev. Lett.*, 85:4637–4640, 2000.

[41] E. Hulata, R. Segev, and E. Ben-Jacob. A method for spike sorting and detection based on wavelet packets and Shannon's mutual information. *J. Neurosic. Methods*, 117:1–12, 2002.

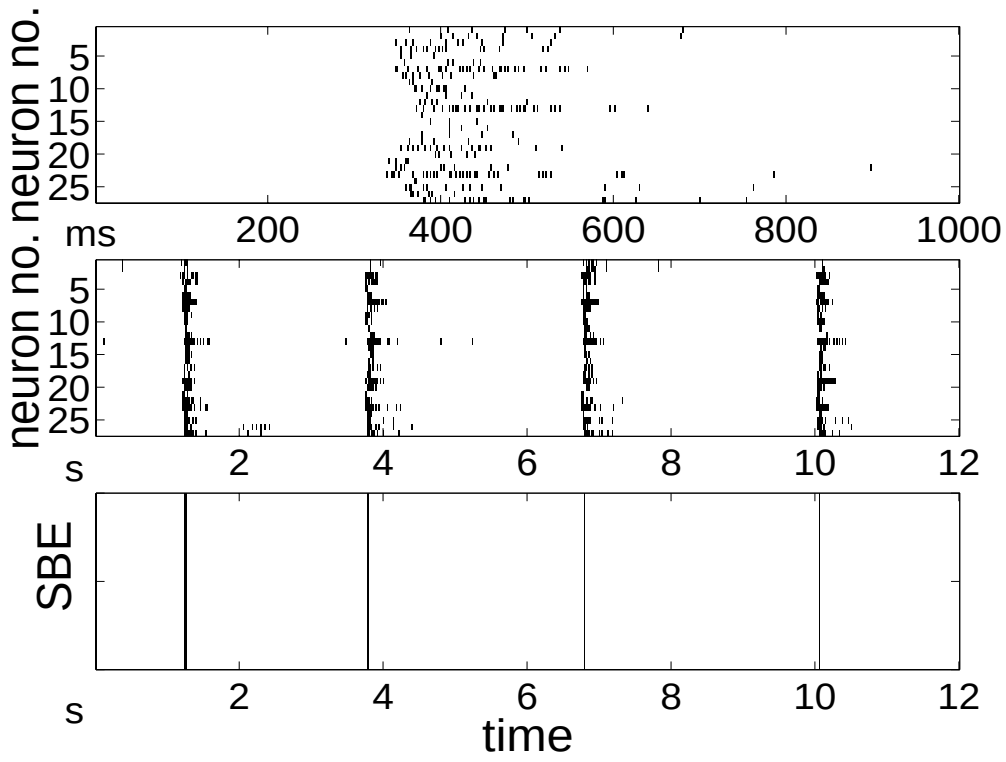

Figure 1:
The formation of a binary sequence from a multi-neuronal recording of an *in-vitro* neuronal network. Top: A raster plot representing the firing events of 27 neurons over a course of 1000msec. For each neuron, a horizontal "bar-code" is plotted where the bars ("1"s) correspond to the location of a single firing event. Middle: A raster plot over a course of 12 seconds. Note that while observing the firing of the network at this larger time scale, it is clear that the firing is characterized by synchronized events, lasting 200msecs. The firing of the top figure is the third synchronized burst (now located at 7secs). Bottom: The synchronized bursts events (SBEs) are easily identified and thus the network's sequences can be transformed into a a new binary sequence. In this sequence, the bars ("1"s) correspond to the locations of the SBEs and the width of the SBEs sets the basic time bin.

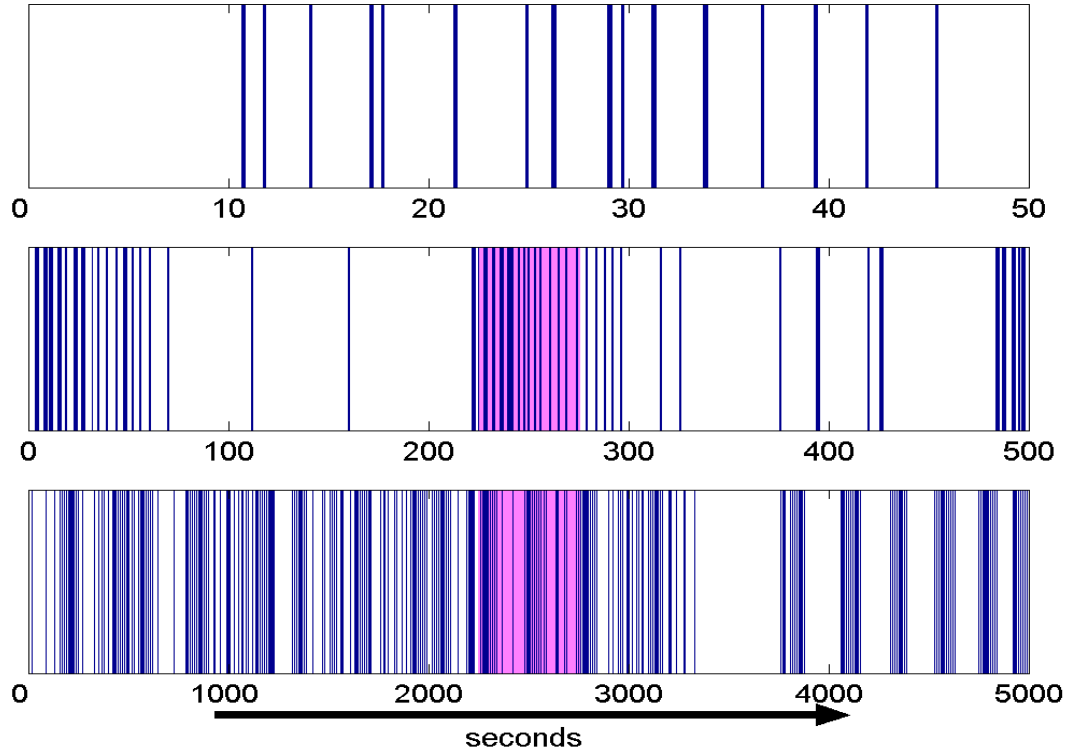

Figure 2:
Recorded electrical activity of *in-vitro* neuronal networks presented via binary time series of their synchronized bursting events (SBEs). The latter are short ($\sim 100ms$) events of rapid firing of about all the neurons. Each one is presented by a bar or 1 on a single time bin. The recorded sequence is presented on three time scales each is composed of 500 time bins which are 100ms, 1s, and 10s respectively from top to bottom. Note that each time scale is presented on the next level by the colored area at the middle. The time series has an hierarchical temporal organization i.e. the SBEs form clusters that on the higher level form clusters of clusters and so on [16]

Figure 3:
Top. A temporal binary sequence of recorded synchronized bursting events (SBE) of an *in-vitro* neuronal network [16]. The original recorded sequence is at time bins of $0.1ms$. This sequence is then scaled to time bins of $400ms$ that correspond to the width of the neuronal SBE of rapid network activity. Consequently, it is turned into a binary "bar-code" representation of the SBE location. The segment shown here is of length $800sec$ ($N_{bin} = 2048$). Bottom. A scrambled binary sequence produced by randomly shuffling the order of the inter-event intervals. It is clear that the distinct segments of the original sequence are smeared.

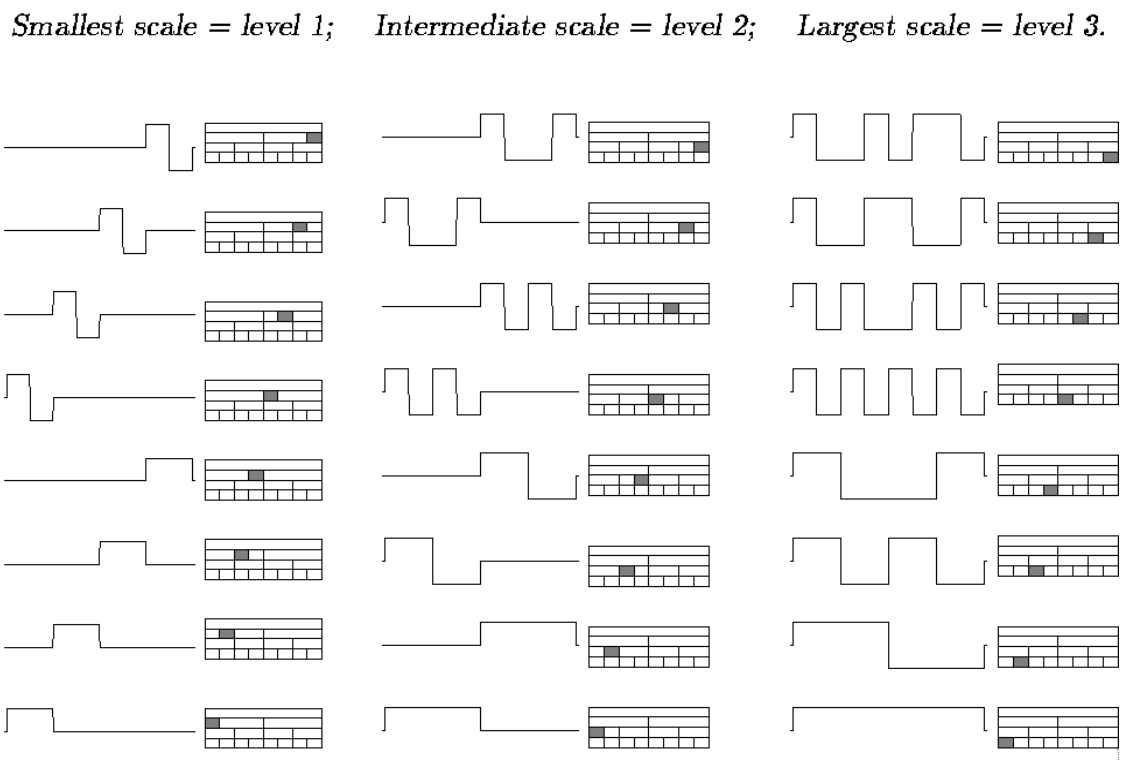

Figure 4:
A demonstration of the time-frequency behavior of different wavelet packets. The mother wavelet used in this case is the simple *Haar* wavelet. In this example there are 8 samples, and thus there are 3 scales of decomposition. All the possible wavelet packets are presented, and each is labeled by the triplet $\psi_{i,j,k}$. In the left column, the packets of scale $i = 1$ are presented. The bottom four packets are the 4 translated packets of block $j = 0$ (low frequencies), and the top four are the packets of block $j = 1$ (high frequencies). In the middle column ($i = 2$), two translated packets of the four frequency blocks $j = 0, 1, 2, 3$ are presented from bottom to top. The right column is the last level of decomposition ($i = 3$), and thus represents the frequency domain. The 8 packets present the 8 possible periods. This figure is adapted from [28]

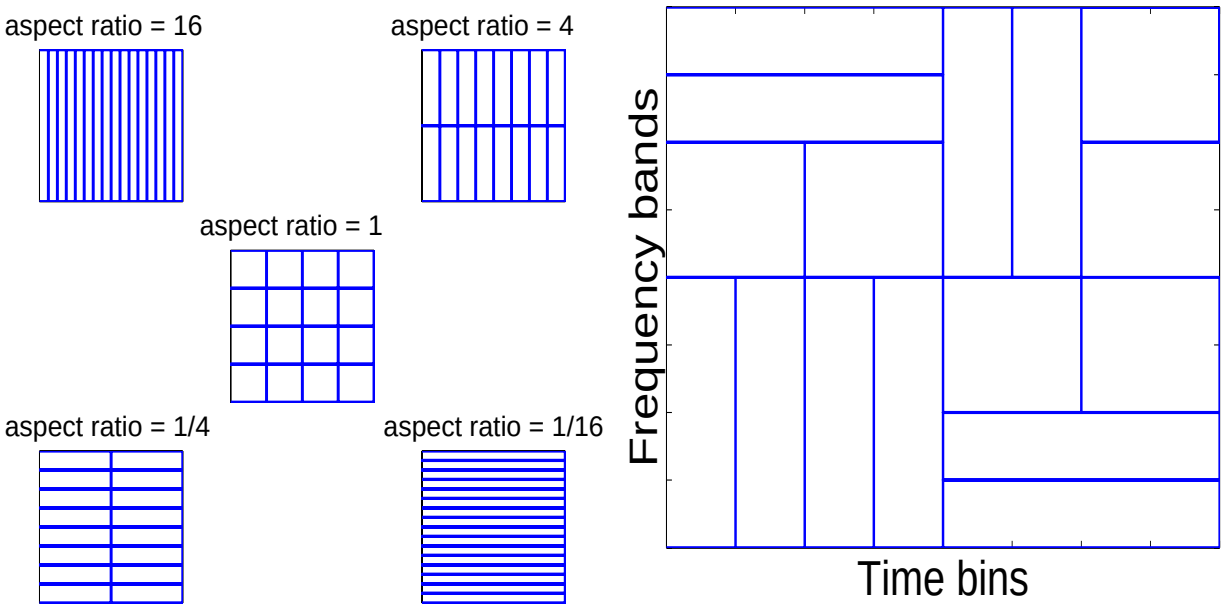

Figure 5:
Example of the 5 possible divisions of a sequence of a length $N_{bin} = 16$ (where each bin is of width $\tau_{bin} = 1$ and the temporal length T is defined by $T = N_{bin}\tau_{bin}$). Left: the top left layer is covered by rectangles with aspect ratio of N_{bin}, which represent the highest time resolution (Δt_{min} is equal to τ_{bin}). The lower right layer is covered by rectangles with aspect ratio of $1/N_{bin}$, which correspond to the highest frequency resolution ($\Delta f_{min} = 1/(N_{bin}\tau_{bin})$. Note that the minimal resolution in time, Δt_{min}, and in frequency, Δf_{min} satisfy $\Delta t_{min} = 1/\Delta f_{max}$ and $\Delta f_{min} = 1/\Delta t_{max}$ respectively. For a signal of length N_{bin} there are $log_2(N_{bin})+1$ different rectangles' aspect ratios.
Right: A typical Best Tiling. The tiling of the time-frequency plane is comprised of N_{bin} packets with various aspect ratios. The best tiling is selected in stages. First, pairs of horizontally adjacent packets from each layer are compared with the corresponding vertically adjacent packets of the next layer. The pair that has the lower sum of M is selected (see Eq. 1). The same procedure is followed for all layers. Next, selected pairs of adjacent packets are combined into tiles of twice the area and with values according to the pairs' sums of M. The first procedure presented above is performed on the newly constructed tiles and so on until one tile covers the entire plane. The individual packets that configure this tile as selected during the different cycles compose the *Best Tiling* [30].

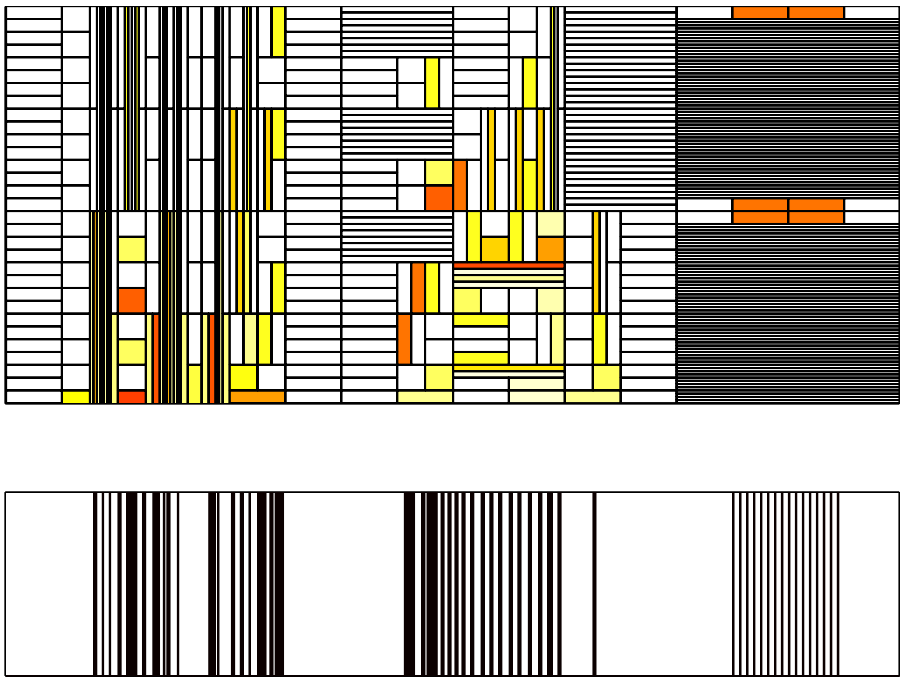

Figure 6:
A Best Tiling representation of a binary sequence. At the bottom we present a binary signal, which is comprised of different types of signals: an artificial periodic sequence (at the right), a sequence from neuronal network's SBE sequences (at the middle) and a sequence comprised of the randomly shuffled intervals of the SBEs (at the left). Note that the middle area of interest, with a unique ordered sequence of 1s, is tiled in a non-trivial way, *i.e.* a mixture of packets' with more various aspect ratios. On the other hand, in the randomly shuffled sequence adjacent tiles tend to be more similar and the periodic segment is tiled in a very uniform and straight forward manner.

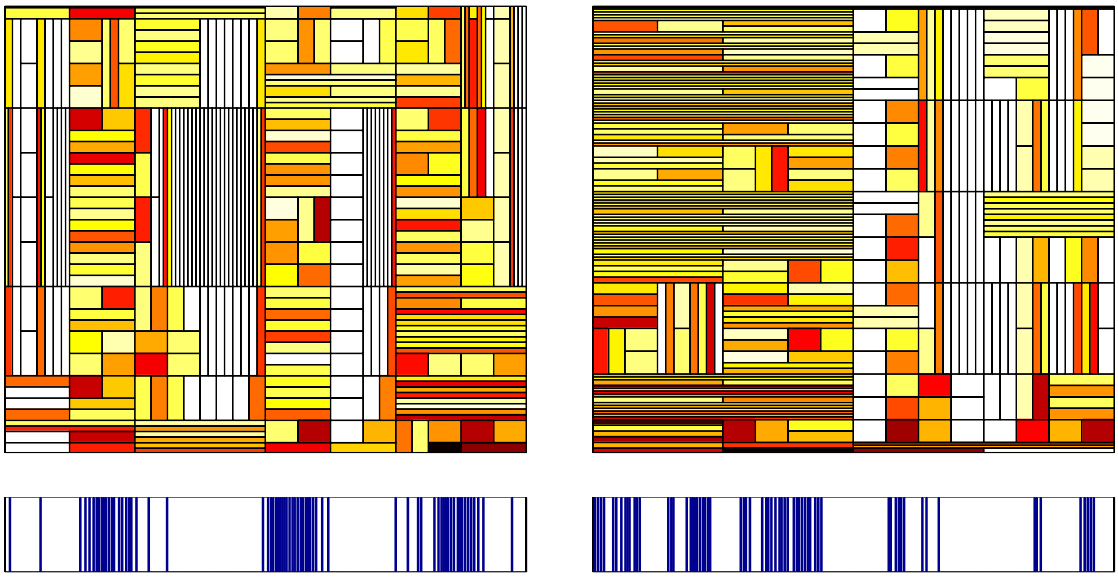

Figure 7:
Temporal binary sequences (bottom) and their corresponding tiled time-frequency planes (top). The SBE binary sequence (left) and the shuffled binary sequence (right) are correspondingly the top and bottom sequences from Fig. 3.
Left. A temporal sequence of recorded synchronized bursting events (SBE) of an *in-vitro* neuronal network [16]. The segment shown here is of length $800sec$ ($N_{bin} = 2048$). In the above time-frequency plane, the horizontal axis is the time domain and the vertical axis is the frequency domain. The color of each rectangle represents the value of its corresponding q_n. The color code ranges from white to red, the highest energy. It should be visible that the tiling of the plain follow the temporal location of the bursting regions while creating a complex pattern with different aspect ratio of tiles.
Right. The corresponding scrambled sequence and its time-frequency plane. The inter-events intervals of the neuronal sequence are randomly shuffled. It is clear that the distinct segments of the original sequence are smeared, and that a larger portion of the time-frequency plane is tiled by neighboring tiles with equal aspect ratio.

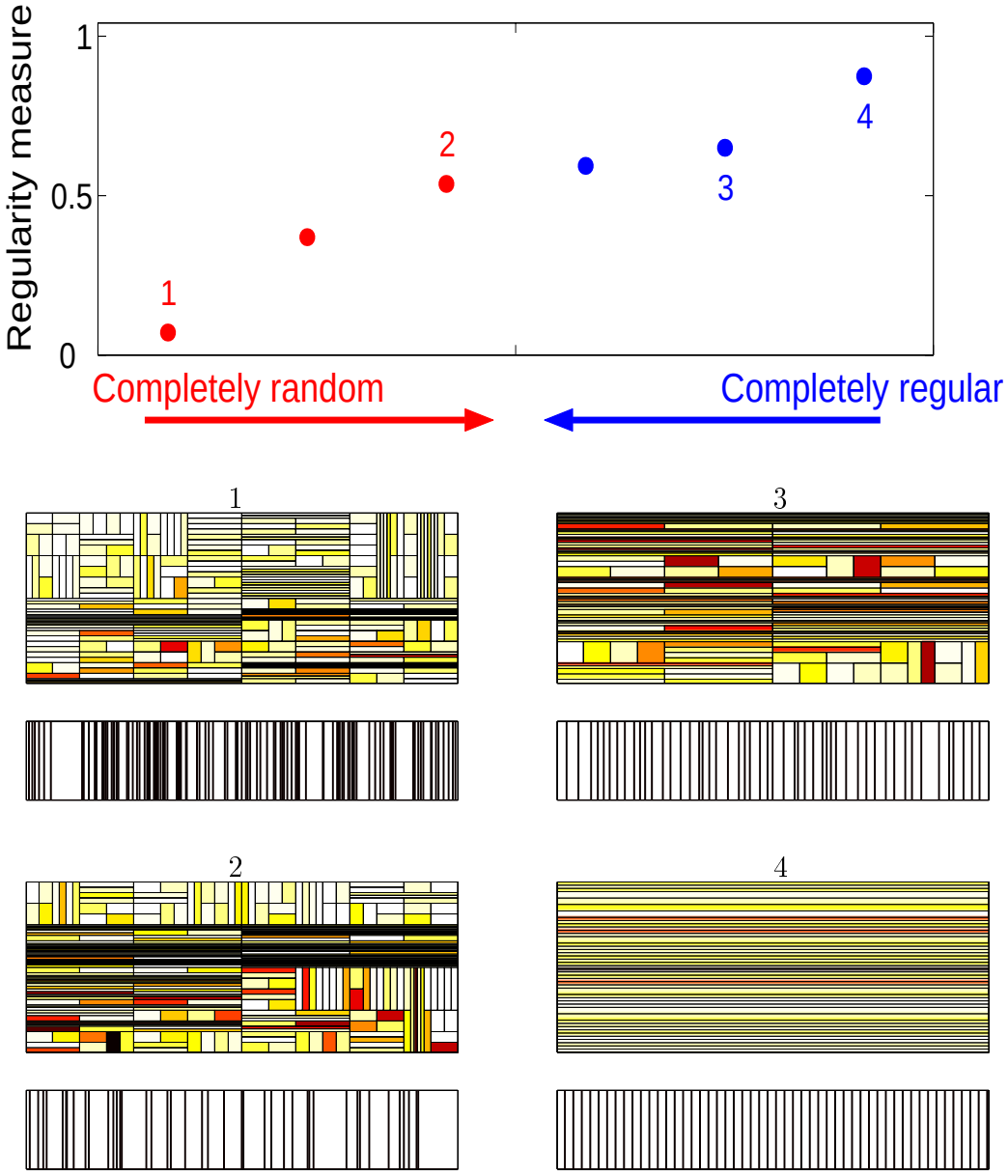

Figure 8:
At the bottom we present four examples of binary sequences, from the artificially constructed family of signals, and their Best Tilings. The signals are labeled 1 to 4, where 1 is a random signal and 4 is a periodic one. Above we present the regularity measure RM (Eq. 3) of the tilings. Note that the RM of the random signal is close to zero, and that of the periodic signal is close to 1.

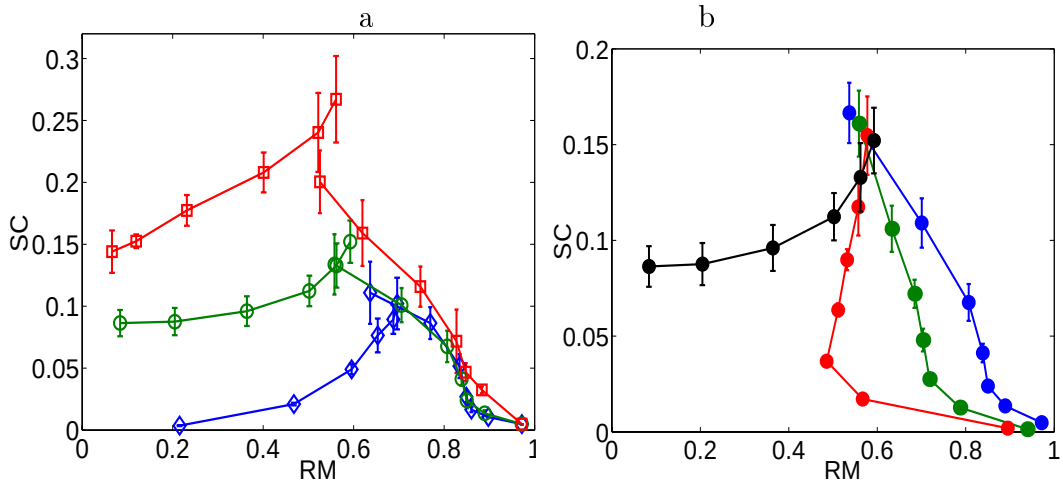

Figure 9:
Characteristics-map for families of artificially constructed sequences of intervals with both zero mean and finite-mean symmetric Lévy distributions. Numerous realizations were constructed for each set of Lévy parameters (α, γ and δ), and we present $\overline{RM}$ and $\overline{SC}$ using $std(RM)$ and $std(SC)$ as errorbars. Left: Three families for $\alpha = 2.0; 1.6$ and 1.2 on both the random and regular sides ($\delta = 0$ and 20 respectively). The variable γ is used to span each characteristic. For random ones, it spans from low regularity at $\gamma = 1$ towards higher regularity and higher complexity with increasing γ. For regular characteristics, $\gamma = 1$ corresponds to high regularity ($RM \to 1$) and increasing of γ lowers the regularity while increasing the complexity. For a given α the regular branches ($\delta \neq 0$) meet the random branch ($\delta = 0$) at high complexity and intermediate regularity. Right: The behavior of the regular branches for the same α and different $\delta = 5, 10, 20$. For comparison, the random branch with the same α and $\delta = 0$ is also plotted. Note that all the regular branches meet together at the same location where the random branch crosses.

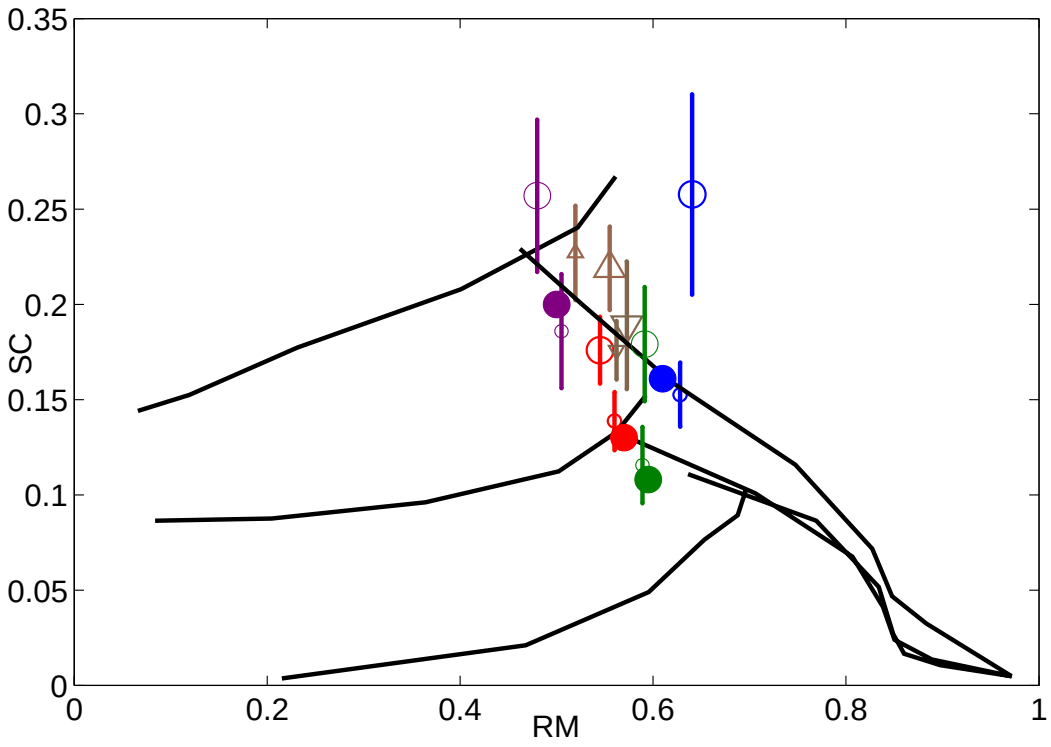

Figure 10:
Utilizing the complexity plane to study recorded neuronal activity and simulated sequences. The solid black characteristics are those presented in the left side of figure 9. The large blue circle represent the $\overline{RM}$ and $\overline{SC}$ of different segments of an *in-vitro* experiment of 10,000 neurons (over the course of an hour). The corresponding errorbars represent $std(SC)$. The smaller blue circle represent the mean values assigned for different shufflings of each of the segments. The blue solid circle indicates the behavior of the artificial set of parameters that were fitted to the distribution of the recorded intervals [16]. Note that the shuffled sequences are repositioned very closely to the corresponding artificial sets. In red, green and purple circles, we present similar sets for different experiments (networks of different number of neurons: 50, 10,000 and 1,000,000 respectively). In brown, we present two sets of simulations with similar time scales. The large triangles represent the RM and SC of the simulation output, and the corresponding smaller triangles represent the values assigned for the shuffled sequences.

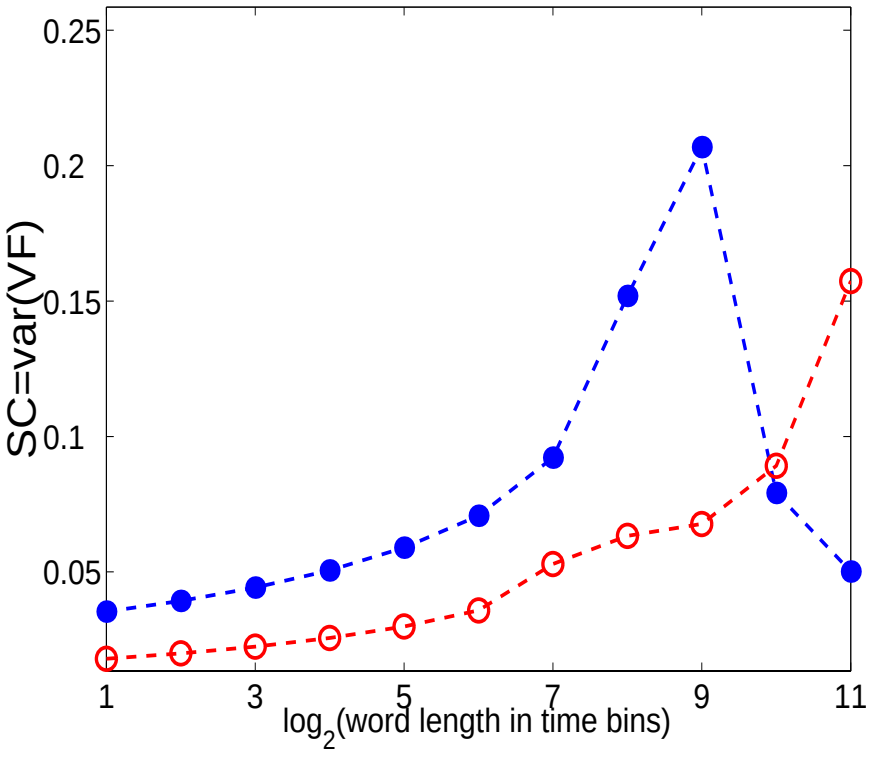

Figure 11:
The variance of the VF as calculated on segments (words) of the signal for different lengths of segments (the log_2 of the length is the horizontal axis). The dots are for a recorded time series of neuronal networks electrical activity as in Fig. 3. The circles are for a constructed signal with no hierarchical temporal organization. The peak for the neuronal time series at word length of $2^9 = 512$ indicates the crossing to the next level of temporal organization.